frontiers | Frontiers in Physics

TYPE Original Research
PUBLISHED 26 January 2026
DOI 10.3389/fphy.2025.1757118

Check for updates

OPEN ACCESS

EDITED BY
Nirpendra Singh,
Khalifa University, United Arab Emirates

REVIEWED BY
Njitacke Tabekoueng Zeric,
University of Buea, Cameroon
Gaurav Jayaswal,
Indian Space Research Organisation, India

*CORRESPONDENCE
Ghada A. Khouqeer,
gkhouqeer@imamu.edu.sa

RECEIVED 29 November 2025
REVISED 23 December 2025
ACCEPTED 24 December 2025
PUBLISHED 26 January 2026

CITATION
Pahari P, AbdelAll N, Mohapatra SK, Das JK and Khouqeer GA (2026) Impact of structural and material parameters on sensitivity of engineered N-pocket DGTFET biosensors. *Front. Phys.* 13:1757118.
doi: 10.3389/fphy.2025.1757118

COPYRIGHT
© 2026 Pahari, AbdelAll, Mohapatra, Das and Khouqeer. This is an open-access article distributed under the terms of the Creative Commons Attribution License (CC BY). The use, distribution or reproduction in other forums is permitted, provided the original author(s) and the copyright owner(s) are credited and that the original publication in this journal is cited, in accordance with accepted academic practice. No use, distribution or reproduction is permitted which does not comply with these terms.

Impact of structural and material parameters on sensitivity of engineered N-pocket DGTFET biosensors

Pallabi Pahari[1,2], Naglaa AbdelAll[3], Sushanta Kumar Mohapatra[2], Jitendra Kumar Das[2] and Ghada A. Khouqeer[3]*

[1]Department of Electronics and Communication Engineering, Haldia Institute of Technology, Haldia, India, [2]School of Electronics Engineering, Kalinga Institute of Industrial Technology (KIIT) Deemed to be University, Bhubaneswar, Odisha, India, [3]Physics Department, Faculty of Science, Imam Mohammad Ibn Saud Islamic University (IMSIU), Riyadh, Saudi Arabia

Biosensors play a crucial role in medical, agricultural, food, and environmental monitoring, where high sensitivity and label-free detection are essential. Conventional FET-based biosensors exhibit limitations including elevated subthreshold slope, leakage current, and inadequate detection of neutral biomolecules. Tunnel FETs (TFETs) utilise a band-to-band tunnelling mechanism, providing steep switching characteristics and low-power operation; however, their practical application is constrained by low ON-current and ambipolar conduction issues. This study proposes and analyses a material developed double-gate TFET featuring an N-pocket and AlGaAs-based heterostructure, utilising Silvaco ATLAS simulations to enhance biosensing capabilities. The device incorporates GaSb–AlGaAs–GaAs heterostructures, dual-gate control, bilayer dielectrics, and optimised doping profiles to enhance tunnelling efficiency and sensitivity. The results indicate that the proposed design attains a subthreshold swing of 9.2 mV/dec, an I_{on}/I_{off} ratio of 4×10^{13}, and a reduced threshold voltage of 0.32 V, surpassing traditional silicon-based and non-pocket devices. Sensitivity analysis indicates a notable improvement with rising dielectric constant, molar fraction and positive biomolecule conditions, whereas negative biomolecules diminish sensitivity as anticipated due to repulsive interactions. The N-pocket DGTFET exhibits stable and reproducible sensitivity relative to conventional and pocket-less devices, with a doping dimension of 3 nm × 10 nm providing an optimal balance between sensitivity and stability. The device demonstrates a significant enhancement in selectivity, achieving sensitivity values of up to 1.20×10^5, which exceeds the performance of previously reported TFET biosensors by multiple orders of magnitude. The findings demonstrate that the modified DGTFET serves as a reliable, energy-efficient, and highly sensitive platform for label-free biomolecule detection.

KEYWORDS

bilayer dielectrics, biosensors, DGTFET, DM-TFET, dual-gate control, FET-based biosensors, GaSb–AlGaAs–GaAs heterostructures, ME-DG-TFET

1 Introduction

In today's world, biosensors have achieved enormous significance in the fields like food industry, medical sector, agriculture, environmental monitoring and forensic sciences [1, 2]. Biosensor is an analytical device that uses biological components (e.g., enzymes, antibody, DNA, etc.) coupled to a transducer (electrical, optical, mechanical, etc.) to convert a specific biological interaction into a measurable signal. The first biosensor was prepared by Clark et al. in 1962 [3], who is also considered as the father of biosensors. Since then researchers are trying to develop well-grounded and error free biosensor for offering label free detection, high sensitivity, scalability and less power consumption [4, 5].

In recent years, substantial progress has been made in the development of ultrasensitive chemical and electrochemical biosensors, particularly for food safety and environmental applications. For instance, advanced electrochemical sensors based on metal–organic framework (MOF)-derived porous composites have demonstrated nanomolar-level detection of organophosphorus pesticides with excellent reproducibility and wide linear ranges [6]. Similarly, AI-assisted colorimetric sensor arrays employing nanozyme-based supramolecular assemblies have enabled sub-micromolar pesticide detection with high classification accuracy, leveraging machine-learning-driven signal processing [7]. While these approaches provide outstanding analytical performance, they often rely on complex material synthesis routes, enzymatic activity control, or external data-processing frameworks, which can limit long-term stability, integration, and miniaturization.

Biological recognition strategies such as aptamer-based sensing have also emerged as powerful tools for highly selective detection of bacteria and other pathogens. Aptamers offer high binding affinity, tunability, and chemical stability, enabling diverse optical and electrochemical transduction schemes. Recent reviews highlight significant advancements in aptamer selection, signal amplification, and sensor robustness, particularly for bacterial detection [8]. However, these systems often involve intricate biochemical functionalization steps and can be sensitive to environmental variations, posing challenges for reproducibility and large-scale integration.

The demand for real-time and wearable biosensing platforms has further accelerated the development of integrated microfluidic and electrochemical devices. Fully integrated wearable microfluidic electrochemical sensors have demonstrated continuous monitoring of multiple sweat biomarkers with near-Nernstian sensitivity and strong mechanical robustness [9]. Despite their practical applicability, such platforms typically require sophisticated packaging, bonding techniques, and multi-layer integration, which can increase fabrication complexity and cost.

At the Frontier of ultra-sensitive diagnostics, CRISPR-based and plasmonic sensing platforms have achieved femtomolar-level detection of viral nucleic acids with exceptional specificity, enabling rapid identification of viral variants [10]. While these systems represent a breakthrough in molecular diagnostics, they rely on optical instrumentation, biochemical reagents, and multi-step assay procedures, which may hinder their adoption in compact, low-power, and scalable electronic sensing systems.

The advantages of field effect transistor (FET) based biosensors including label free operation, high sensitivity, low-power consumption, CMOS compatibility and the potential for large-scale integration, have drawn a lot of interest in recent years for the detection of biomolecules [11–14]. These devices use bio-receptors to functionalise the oxide layer or dielectric cavity. The interaction of biomolecules creates a gating effect that modifies the electrical properties of the device, allowing for detection. Short Channel effects (SCEs), leakage current, subthreshold slop (SS) restricted to > 60mV/dec by the thermionic emission limit and weak detection of neutral biomolecules are some of the disadvantages of conventional FET biosensor [15]. In real world applications, these problems limit their maximum sensitivity and selectivity. Because of their subthreshold slope below 60mV/dec, ultra-low leakage current and steep switching characteristic, TFETs have become a promising option for next-generation biosensing applications [16, 17]. TFETs rely on the band-to-band tunnelling (BTBT) mechanism [18, 19], which allows for quick response times, low voltage operation and better sensing performance than MOSFETs which use thermionic emission to control current flow.

TFET biosensors have limitations despite these advantages. Practical implementation is hampered by their ambipolar conduction and relatively low ON current [I_{on}] [20, 21]. Multiple engineering techniques, such as heterogate architectures, high-K dielectric stacks, high band gap channel material [22]. Moreover, dielectrically modulated TFET biosensors have been developed as a result of the integration of DM with FET structure [23–27]. This topology increases device sensitivity by regulating the drain current through the insertion of biomolecules with different dielectric constants or charges into the nano-gap cavity close to the gate. Selectivity (ΔS) differentiates between distinct biomolecules, whereas sensitivity(S) measures the capacity to detect the presence of biomolecules [28]. Because the can detect both charged and neutral biomolecules, operate at lower supply voltages and achieve higher sensitivity, DM-TFET biosensors [25–27]. To ensure accurate and robust detection of a broad range of biomolecules, there is still a plenty of scope to improve sensitivity and selectivity. Based on these designs, this work suggests and investigates sophisticated DM-TFET architectures designed for high-performance biosensing uses.

2 Models and methods

The standard silicon-based Tunnel FET (TFET) has low tunnelling efficiency and poor performance in the subthreshold range. The concept for Material Engineered Double Gate TFET (ME-DG-TFET) fixes these problems by using a heterostructure comprising three compound semiconductors shown in Figure 1. The channel is made out of a ternary compound semiconductor ($Al_{0.47}Ga_{0.53}As$). The source is Gallium Antimonide (GaSb) with a low bandgap of 0.72 eV to make band-to-band tunnelling easier, while the drain is Gallium Arsenide (GaAs). The source, channel, and drain are doped with p++ (1×10^{20} cm^{-3}), n (1×10^{17} cm^{-3}), and n+ (5×10^{18} cm^{-3}), respectively. A 3 nm n + pocket with a doping of 5×10^{19} cm^{-3} is added near the source-channel junction to make the tunnelling width smaller and the ON-current stronger. The 50 nm long channel is covered by a bilayer gate dielectric stack made up of 0.5 nm SiO_2, which protects against leaks and makes

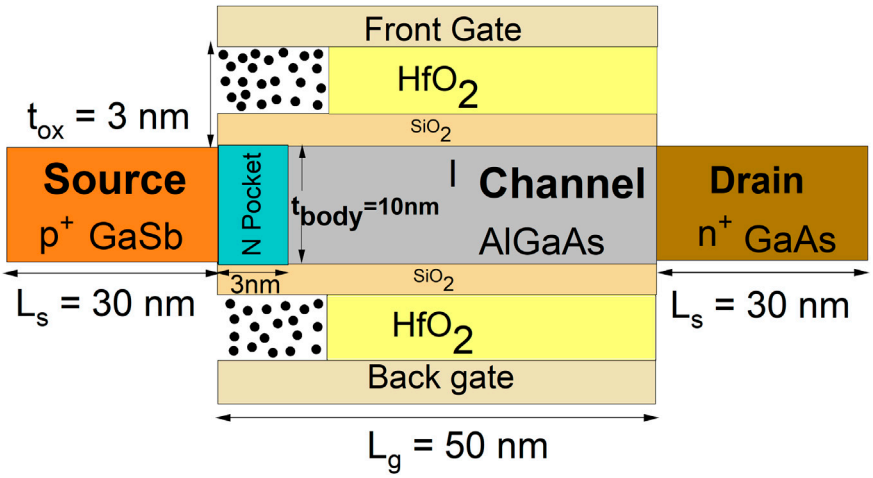

FIGURE 1
Modified DGTFET structure with cavity.

TABLE 1 Parameter specification of device.

Parameter	Value
Channel length	50 nm
T_{si}	10 nm
$T_{ox}(SiO_2+HfO_3)$	3 nm
Source length	30 nm
Drain length	30 nm
Source doping (P+)	1×10^{20}
Channel doping(I)	1×10^{17}
Drain doping (N+)	5×10^{18}
N+ pocket doping	5×10^{19}

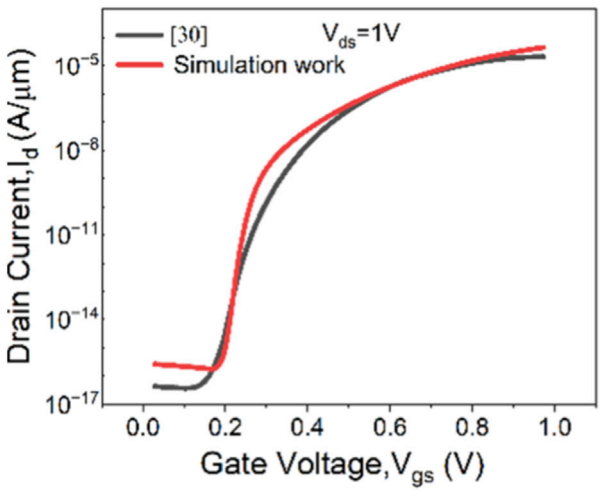

FIGURE 2
Calibration of TFET structure through Ref. [30].

the gate more sensitive, and 1.5 nm HfO_2, which makes the gate more powerful. Both gates have a work function of 4.0 eV. There are also 15 nm × 1.5 nm cavities made near the source-channel junction which can sense biomolecules, which allows for biosensing. In general, this method of material and structural engineering using GaSb–AlGaAs–GaAs heterostructures, pocket doping, dual-gate control, and bilayer dielectrics greatly improves tunnelling efficiency, ON-current, and sensitivity. This makes the ME-DG-TFET better than the regular Si-based TFET. The device parameters are listed in Table 1.

All simulations were done in Silvaco Atlas [29]. The calibration of the TFET simulation shown in Figure 2. The simulations use a very fine mesh across the region where the tunneling takes place, from which energy band profiles and the energies for which band-to-band tunneling is permitted, are determined. To calculate the tunneling current we use non-local band-to-band tunneling (BTBT) also use the band gap narrowing (BGN) model to utilize the highly doped regions in the device. In the simulation, the Shockley- Read-Hall (SRH) and Auger models are considered to evaluate generation/recombination. In addition, the Fermi-Dirac distribution function model and the drift–diffusion carrier transport model are also employed in the simulation. Concentration-dependent mobility mode is incorporated by conmob, also concentration-dependent lifetime is incorporated by consrh.

Table 2 shows the comparison of the conventional silicon-based DGTFET, without N-pocket group III-V based DGTFET and the suggested DG-TFET at a gate length of 50 nm. It shows that the DG-TFET has far better electrostatic and transport properties. Figure 3 shows the suggested device's subthreshold swing (SS) has been greatly lowered from 31.4 mV/dec to 9.6 mV/dec. This shows that the gate control is better and the switching is sharper. The ON-state current (I_{on}) goes up a little from 3.5×10^{-5} and far from 1.48 ×

TABLE 2 Performance comparison between three different structures.

Parameters	Modifications of DGTFET structure with L_G = 50 nm		
	Silicon based	Without N-pocket	This work
SS(mV/dec)	31.4	10.7	9.2
I_{on} (A/μm)	5.91×10^{-5}	1.48×10^{-6}	3.5×10^{-5}
I_{off} (A/μm)	2.68×10^{-16}	1.67×10^{-18}	8.8×10^{-18}

10^{-6} in the silicon version to 5.9×10^{-5} A in the designed and without N-pocket version respectively. I_{off} is significantly decreased from 2.68×10^{-16} A to 8.8×10^{-18} A, which is essential for low-power functionality. So, the I_{on}/I_{off} ratio goes up from 2.2×10^{11} and 8.86×10^{11} to 4×10^{13}, which is over two orders of magnitude better. This makes switching more reliable and less sensitive to noise. Also, the threshold voltage (Vth) the operating voltage is lower and the energy efficiency is better as the voltage drops from 0.46 V to 0.32 V. All of these performance gains show how well material and structural engineering work in the modified DG-TFET. This makes it a good choice for future ultra-low-power and high-performance nanoelectronics applications.

The energy band diagram in Figures 3e–g illustrates that, because of its larger bandgap and gradual band bending, the silicon DGTFET has a wide tunneling barrier at the source-channel junction, which corresponds to a low probability of tunneling and reduced ON-state current. In the DGTFET without an N-pocket, the steeper band bending narrows the tunneling barrier; without proper electrostatic regulation, however, the tunneling junction may be highly sensitive even to minor perturbations, resulting in unstable and non-physical current amplification. In contrast, a narrow tunneling barrier is created in the DGTFET with an optimized N-pocket, but it is well-controlled, enhancing band-to-band tunneling while maintaining electrostatic stability and hence achieving high and physically consistent device performance.

3 Results and discussions

3.1 I_d-V_{gs} of modified DG-TFET for charged biomolecules

The transfer characteristics of the designed DG-TFET under V_{ds} = 1V in Figure 4 shows how the charge density and dielectric constant of biomolecules affect how well a device works. For biomolecules with a positive charge (N_{bio} (C/cm^2) >0), When the biomolecule concentration increases (K = 12), the drain current shows a significant increase. This is because the extra positive charge narrows the tunneling barrier, which increases the band-to-band tunneling probability and causes the subthreshold slope to become steeper and the I_{ON} to rise. Compared to the baseline device (K = 1, N_{bio} = 0).

On the other hand, biomolecules with a negative charge (N_{bio} < 0, K = 12) stops the tunneling current, moving the transfer characteristics toward higher gate voltages and lowering I_{on} because the tunneling barrier has been made wider. Also, when there are no biomolecules (N_{bio} = 0), the dielectric constant's change shows that a rise in K greatly improves the electrostatic coupling between the gate and channel, resulting in higher drain currents and a faster switching response. In summary, these results show that the modified DG-TFET is very sensitive to changes in the polarity and density of biomolecular charges, as well as to changes in the dielectric environment. This confirms its potential as an ultra-low-power and high-performance platform for label-free biomolecule detection.

3.2 Sensitivity analysis with different aspects

3.2.1 Impact of body length variation on sensitivity

The study investigated because of its great sensitivity to electrostatic perturbations, decreased quantum confinement effects, and balance between fabrication reproducibility, a reference body length of 10 nm was chosen. The validation results, which are expressed in terms of ln values as shown in Figure 5, clearly show how charge polarity has a significant impact on biomolecular body length. The baseline was established for neutral biomolecules (N_{bio} = 0), where Sensitivity (S_I) values showed a consistent rise with increasing K. S_I values increased from 1.59×10^7 (K = 5) to 9.54×10^7 (K = 12) at t_{body} = 15 nm. For t_{body} = 10 nm ($2.07 \times 10^4 \rightarrow 8.92 \times 10^4$) and t_{body} = 12 nm ($2.01 \times 10^5 \rightarrow 9.43 \times 10^5$), similar progressive increases were noted. S_I values were consistently greater than neutral in the case of positively charged biomolecules (K = 12), demonstrating elongation brought on by attractive electrostatic interactions. Values rose from 9.69×10^7 (K = 5 × 10) to 1.47×10^8 (K = 1 × 12) at t_{body} = 15 nm, but similar positive shifts were seen for t_{body} = 10 nm ($8.46 \times 10^4 \rightarrow 1.20 \times 10^5$) and t_{body} = 12 nm ($9.61 \times 10^5 \rightarrow 1.38 \times 10^6$). On the other hand, contraction brought on by repulsive forces was reflected in suppressed ln values for negatively charged biomolecules (nbio = -ve). The values decreased from 9.25×10^7 (K = 5 × 10) to 5.80×10^7 (K = 1 × 12) at t_{body} = 15 nm. Similar negative trends were seen for t_{body} = 10 nm ($8.33 \times 10^4 \rightarrow 5.50 \times 10^4$) and t_{body} = 12 nm ($9.23 \times 10^5 \rightarrow 6.16 \times 10^5$). All things considered, the research demonstrates that whereas neutral biomolecules scale naturally with K, positive charges encourage elongation and negative charges cause contraction; the degree of divergence increases with increasing K values. These findings confirm the robustness of the suggested concept by highlighting how sensitive nanoscale body length is to electrostatic conditions.

3.2.2 Impact of molar fraction variation on sensitivity

Figure 6 shows how sensitivity changes with different molar fractions (Al_x, x = 0.3, 0.4, 0.5) when biomolecules are neutral, positively charged, or negatively charged and K values are different. The results show how both compositional tweaking and electrostatic interactions affect the sensitivity of the device. For the neutral system, sensitivity increased consistently with both molar fraction and K. Values at $Al_{0.3}$ went from 1.00×10^2 (K = 5) to 2.98×10^2 (K = 12). For $Al_{0.4}$, the sensitivity went up from 2.07×10^4 to 8.92×10^4. For $Al_{0.5}$, it went up even more, from 3.47 ×

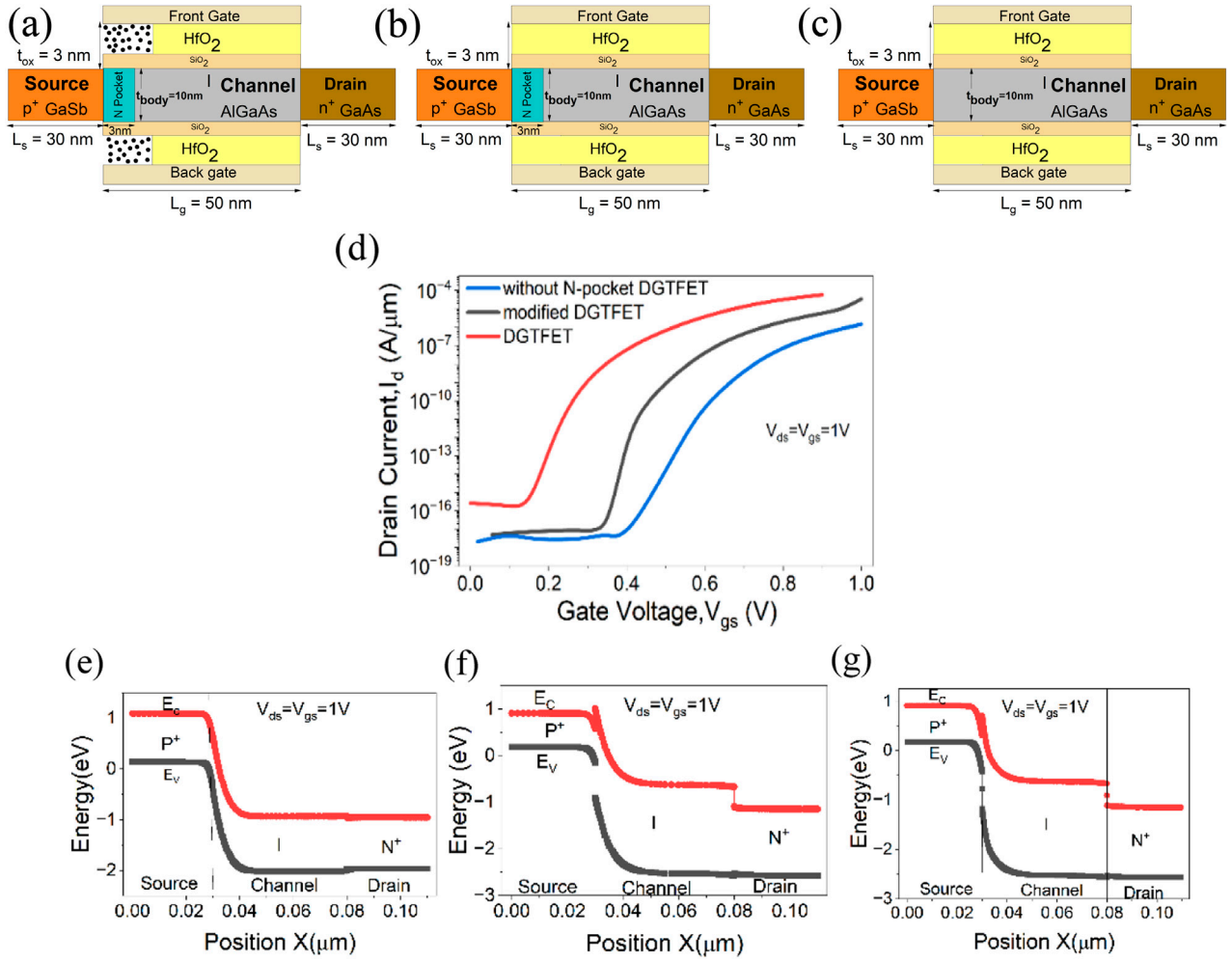

FIGURE 3
Device structure **(a)** Si based DGTFET, **(b)** without N-pocket DGTFET, **(c)** with N-pocket DGTFET and **(d)** I_d Vs. V_{gs} for three different structures, **(e)** EBD of Si based DGTFET, **(f)** EBD of without N-pocket DGTFET, **(g)** EBD with N-pocket DGTFET in ON state.

10^5 to 2.10×10^6. This steady rise proves that more Al makes things more sensitive, since bigger bandgap and dielectric changes make it easier to trap and detect carriers. When using positive biomolecules, the sensitivity values were always higher than when using neutral biomolecules. This proved that electrostatic attraction can increase the response of a device. For Al0.3, sensitivity increased somewhat from 3.02×10^2 ($K = 5 \times 10^{10}$) to 3.20×10^2 ($K = 1 \times 10^{12}$). The improvement was bigger at larger fractions: $Al_{0.4}$ ($8.46 \times 10^4 \rightarrow 1.20 \times 10^5$) and $Al_{0.5}$ ($2.16 \times 10^6 \rightarrow 3.36 \times 10^6$). The trend shows that positive charges work better with increasing Al content, which leads to more carrier modulation and sensitivity. For negatively charged biomolecules, sensitivity levels were diminished compared to neutral ones, validating contraction effects resulting from repulsive interactions. At $Al_{0.3}$, sensitivity dropped from 2.87×10^2 ($K = 5 \times 10^{10}$) to 2.23×10^2 ($K = 1 \times 10^{12}$). At $Al_{0.4}$, the numbers went down from 8.33×10^4 to 5.50×10^4. At $Al_{0.5}$, they went down a lot, from 2.05×10^6 to 1.25×10^6. This downward change is due to charge inhibition and less carrier density modulation when there is a negative charge. The enhanced sensitivity that was seen with more Al is because the bandgap is broader and the dielectric constant changes, which makes it easier to regulate the channel using electrostatics. Higher Al percentages make leakage less likely and improve carrier orientation, which makes the device better at picking up external biomolecular charges. So, $Al_{0.5}$ is the most sensitive, followed by $Al_{0.4}$ and $Al_{0.3}$.

3.2.3 Impact of device architecture on sensitivity (N-pocket vs. conventional vs. without N-pocket)

The influence of device architecture on current sensitivity was examined by comparing the designed DGTFET with N-pocket to the conventional DGTFET and a structure without an N-pocket, under conditions involving neutral, positively charged, and negatively charged biomolecules as shown in Figure 7. The findings consistently indicate that the N-pocket DGTFET yields the most stable and physically relevant sensitivity response, whereas comparable devices either underperform or display unrealistic amplification. Under neutral conditions, the N-pocket DGTFET exhibited a moderate and controlled increase in sensitivity from

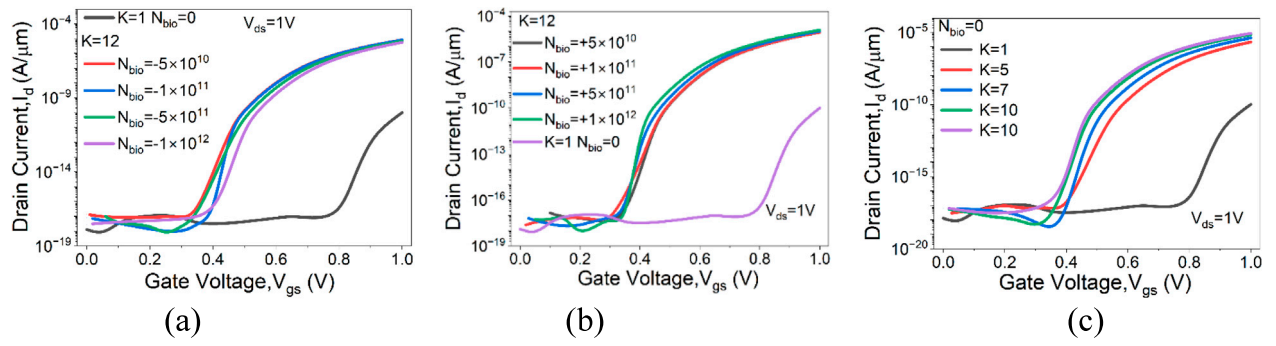

FIGURE 4
I_d-V_{gs} characteristics of modified DG-TFET **(a)** for positive charged biomolecules **(b)** negative charged biomolecules **(c)** for neutral biomolecules.

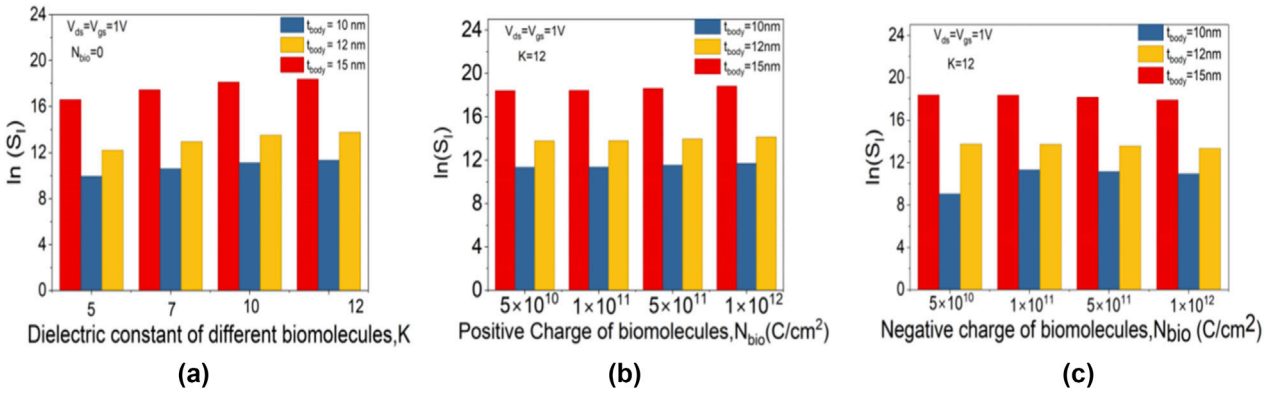

FIGURE 5
Impact of Variation of body length in current sensitivity (S_I) **(a)** for neutral **(b)** for positive charged and **(c)** negative charged biomolecules.

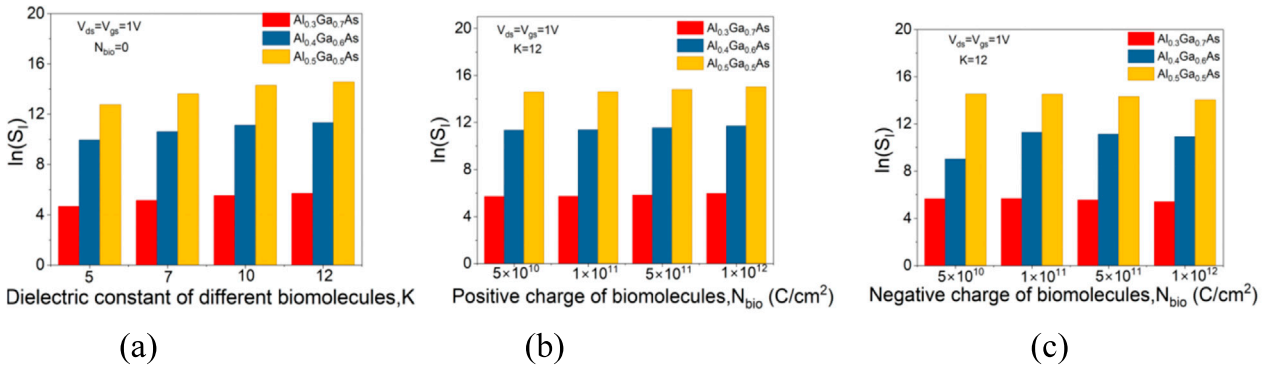

FIGURE 6
Impact of Variation of molar fraction in current sensitivity (S_I) **(a)** for neutral **(b)** for positive charged and **(c)** negative charged biomolecules.

2.07×10^4 (K = 5) to 8.92×10^4 (K = 12). In contrast, the conventional device recorded higher but less controlled values ranging from 1.42×10^5 to 2.86×10^6, while the structure lacking an N-pocket displayed abnormally large values on the order of 10^{11}, indicating instability due to insufficient electrostatic confinement. The N-pocket DGTFET demonstrated a consistent enhancement for positively charged biomolecules, increasing from 8.46×10^4 to 1.20×10^5. In contrast, the conventional DGTFET achieved values in the 10^6 range with reduced tunability, while the device lacking an N-pocket exhibited inflated values surpassing 10^{11}. In the presence of negatively charged biomolecules, the N-pocket DGTFET exhibited a significant reduction in sensitivity from 8.33×10^4 (K = 5×10^{10})

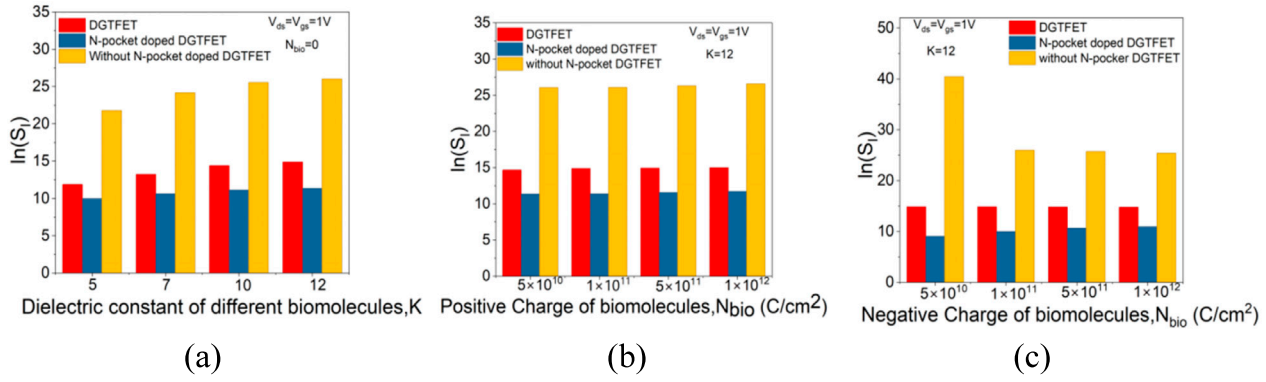

FIGURE 7
Impact of Variation of different structure in current sensitivity (S_I) **(a)** for neutral **(b)** for positive charged and **(c)** negative charged biomolecules.

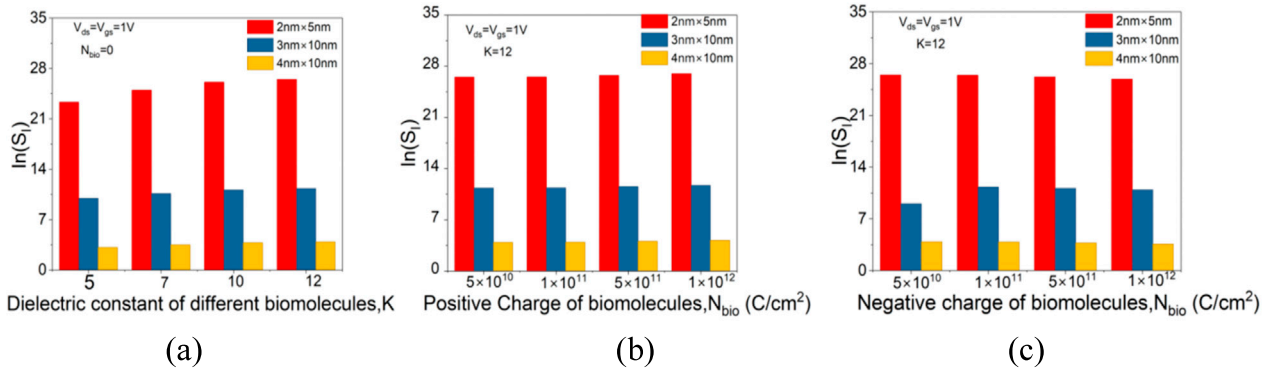

FIGURE 8
Impact of Variation of different dimension of N-pocket in current sensitivity (S_I) **(a)** for neutral **(b)** for positive charged and **(c)** negative charged biomolecules.

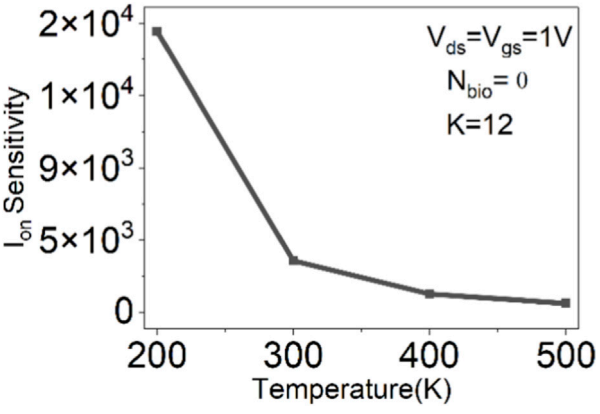

FIGURE 9
Effect of temperature on current sensitivity.

to 5.50 × 10^4 (K = 1 × 10^{12}), consistent with anticipated repulsive interactions. In contrast, the conventional DGTFET displayed only a minor decrease (2.84 × 10^6 to 2.56 × 10^6), while the device lacking an N-pocket demonstrated non-physical responses. The observations support the N-pocket DGTFET as the optimal architecture. The inclusion of the pocket region enhances gate-to-channel coupling, improves charge confinement, and mitigates instability, ensuring that sensitivity is moderate, reproducible, and physically consistent across various biomolecular charge states. Conversely, the traditional device, despite its ability to attain greater magnitudes, exhibits diminished control, and the lack of the N-pocket results in unregulated current amplification. The inclusion of the N-pocket is justified as it achieves a balance between sensitivity and robustness, rendering the DGTFET with N-pocket the most reliable structure for practical biosensing applications.

3.2.4 Impact of N-pocket doping dimension variation on sensitivity

Figure 8 shows the influence of doping dimensions on current sensitivity was examined for structures measuring 2 nm × 5 nm, 3 nm × 10 nm, and 4 nm × 10 nm in the presence of neutral, positive, and negative biomolecules. The findings indicate that while the 2 nm × 5 nm configuration achieves the highest sensitivity (e.g., 1.33 × 10^{10} → 3.13 × 10^{11} for the neutral case), the significantly large values underscore excessive gate-to-channel coupling, potentially

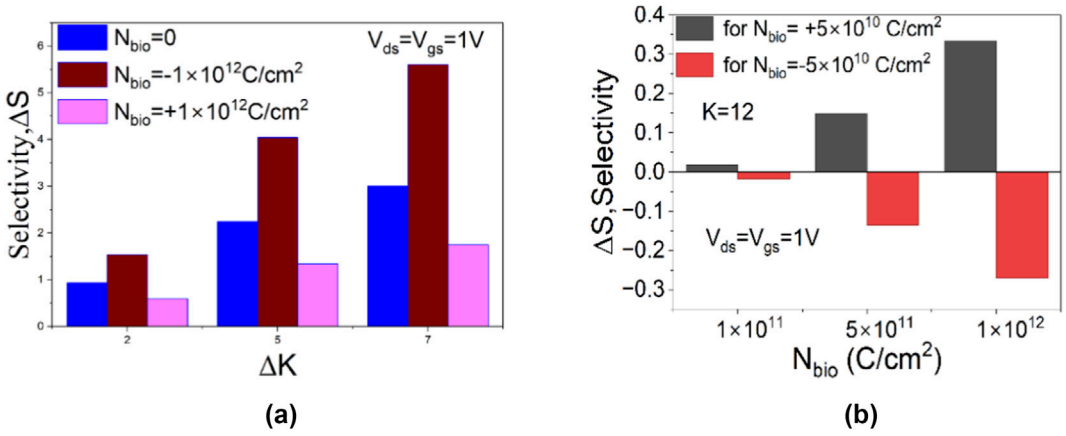

FIGURE 10
(a) Selectivity of DG-TFET biosensor for K = 5, **(b)** N_{bio} = ±5 × 10^{10} C/cm^2.

TABLE 3 Comparative analysis of sensitivity (S_I) with literature.

References	L_g (nm)	V_{ds}/V_{gs} (V)	K	S_I
[17]	50	1/1	10	3.7
[32]	50	0.5/1.5	12	7.3
[33]	50	1/1	12	0.99
[34]	-	-	-	≈10–250
[35]	-	-	-	≈1.1–1.3 p.m./με
[36]	-	-	-	Accuracy ≈ 92–98%
[37]	-	-	-	≈10^2–10^4 A/W
This work	50	1/1	12 (positive)	1.20E+05
This work	50	1/1	12 (negative)	5.50E+04
This work	50	1/1	12 (neutral)	8.30E+04

resulting in instability and poor reproducibility during practical operation. The 4 nm × 10 nm structure exhibited the lowest sensitivity, with values ranging from 2.28 × 10^1 to 4.95 × 10^1 under neutral conditions, indicating diminished electrostatic control and impaired biomolecule detection capability. The doping dimension of 3 nm × 10 nm employed in this study yielded moderate and well-regulated sensitivity, with values spanning from 2.07 × 10^4 to 8.29 × 10^4 for the neutral case, 8.46 × 10^4 to 2.65 × 10^5 for positive biomolecules, and 8.33 × 10^4 to 5.50 × 10^4 for negative biomolecules. The results support the choice of 3 nm × 10 nm as the optimal doping dimension, providing a favourable balance between sensitivity and stability. This dimension is significantly superior to 4 nm × 10 nm for effective biosensing, while also overcoming the non-physical amplification trends observed in 2 nm × 5 nm devices. The choice of doping profile guarantees practical reliability and uniform sensitivity performance under various biomolecular charge conditions.

3.3 Effect of temperature of current sensitivity

Figure 9 shows how the ON-current sensitivity (I_{on}) of the proposed N-pocket DGTFET biosensor with temperature. It is clear from the results that the sensitivity values remain more or less stable with a less fluctuating nature over the tested range of temperatures, which signifies a weak temperature dependence of the tunneling-dominated transport process. Contrary to the temperature-sensitive thermionic emission-dominated transport process in the thermionic emission-based MOSFET biosensor, where sensitivity is meased to be severely decreasing with increasing temperatures, the DGTFET exhibits weak sensitivity variations because of the dominance of the band-to-band tunneling process at the source-channel junction.

3.4 Selectivity analysis

Selectivity is another important part of biosensing. It is the biosensor's response to the target biomolecule compared to other biomolecules. In this study, selectivity is defined as the relative change in the ON current with respect to the target biomolecule having a dielectric constant of 5. Specifically, the selectivity (ΔS) is evaluated as the ratio of the change in ON current to the ON current corresponding to the target biomolecule, where the change in ON current is obtained by subtracting the ON current at a dielectric constant of 5 from the ON current values associated with other biomolecules having dielectric constants of 7, 10, and 12 [31]. Figure 10a describes the variation of selectivity (ΔS) with the change in dielectric constant (ΔK) under differently charged biomolecules (±Nbio), showing that selectivity increases with ΔK and is maximized for negatively charged biomolecules due to stronger modulation of the tunneling current. Figure 10b illustrates the effect of positive and negative biomolecular charges on selectivity at K = 12, representing that positive charges increase selectivity whereas negative charges reduce it, highlighting the robust dependence of device selectivity on charge polarity of biomolecules at Vds = Vgs = 1 V.

Table 3 compares previously reported TFET-based biosensors, which exhibit relatively modest sensitivity values, the modified DG-TFET demonstrates a remarkable enhancement. In this work, the sensitivity reaches 1.20×10^5 for positively charged biomolecules, 5.50×10^4 for negatively charged biomolecules, and 8.30×10^4 for neutral biomolecules under identical device dimensions and biasing conditions. This improvement by several orders of magnitude highlights the effectiveness of the proposed structural engineering, including material heterostructures, dielectric cavity design, and pocket doping, thereby validating the modified DG-TFET as a highly promising candidate for ultrasensitive and label-free biomolecule detection. Dielectric-modulated Schottky-FETs, electrically doped TFETs, and dielectric-engineered Schottky MOSFETs have been explored as label-free biosensors by employing nanogap cavities and dielectric engineering to modulate barrier width, tunneling probability, and device current in response to biomolecules [17, 32, 33]. Recent studies have demonstrated advanced sensing platforms ranging from metal-nanocluster-functionalized SnO_2 nanotube gas sensors achieving ppb-level selective gas detection through catalytic and electronic modulation, to bare fiber Bragg grating sensors enabling real-time monitoring of mechanical stress waves in power semiconductor devices for failure diagnostics [34, 35]. Recent interdisciplinary sensing advances span from multi-sensor fusion–based intelligent assistive systems enabling accurate and adaptive control of power wheelchairs for individuals with disabilities, to twistronics-enabled optoelectronic biosensors that exploit moiré superlattices and plasmonic–CRISPR coupling to achieve ultralow, sub-femtomolar biomolecular detection [36, 37].

4 Conclusion

This work establishes that targeted material and structural optimization significantly enhances DGTFET performance for label-free biosensing. The proposed GaSb–AlGaAs–GaAs heterostructure DGTFET incorporating a bilayer gate dielectric and an N-pocket demonstrates improved electrostatic control and tunnelling efficiency. The device achieves a subthreshold swing of 9.2 mV/dec, an I_{ON}/I_{OFF} ratio of 4×10^{13}, and a reduced threshold voltage of 0.32 V, validating its ultra-low-power operation. Sensitivity values of 1.20×10^5, 8.30×10^4, and 5.50×10^4 are obtained for positively charged, neutral, and negatively charged biomolecules, respectively, at K = 12, outperforming reported TFET biosensors. The N-pocket suppresses non-physical amplification and ensures stable sensitivity trends, while an optimized 3 nm × 10 nm pocket offers the best compromise between sensitivity and robustness. The proposed architecture is therefore well suited for practical biosensing applications. Future work will involve the experimental demonstration of the proposed N-pocket DG-TFET biosensor based on III-V heterostructures to verify the sensitivity trends explored via simulation. The influence of interface states, oxide traps, and process variations will be investigated. Noise analysis, sensitivity, and device stability will be used to establish the lowest detectable concentration of biomolecules. Additionally, sensing dynamics will be explored to assess the feasibility of real-time sensing. Finally, scaling the device architecture and developing a sensor array based on the device will be considered to allow low-power, CMOS-compatible biosensors to be used in large-scale sensing.

Data availability statement

The original contributions presented in the study are included in the article/supplementary material, further inquiries can be directed to the corresponding author.

Author contributions

PP: Methodology, Writing – original draft. NA: Supervision, Validation, Writing – review and editing. SM: Supervision, Writing – original draft. JD: Investigation, Writing – review and editing. GK: Investigation, Writing – review and editing.

Funding

The author(s) declared that financial support was received for this work and/or its publication. This work was supported and funded by the Deanship of Scientific Research at Imam Mohammad Ibn Saud Islamic University (IMSIU) (grant number IMSIU-DDRSP2603).

Conflict of interest

The author(s) declared that this work was conducted in the absence of any commercial or financial relationships that could be construed as a potential conflict of interest.

The reviewer GJ declared a past co-authorship with the author GK to the handling editor.

Generative AI statement

The author(s) declared that generative AI was not used in the creation of this manuscript.

Any alternative text (alt text) provided alongside figures in this article has been generated by Frontiers with the support of artificial intelligence and reasonable efforts have been made to ensure accuracy, including review by the authors wherever possible. If you identify any issues, please contact us.

Publisher's note

All claims expressed in this article are solely those of the authors and do not necessarily represent those of their affiliated organizations, or those of the publisher, the editors and the reviewers. Any product that may be evaluated in this article, or claim that may be made by its manufacturer, is not guaranteed or endorsed by the publisher.

References

1. Ghosh S, Chattopadhyay A, Tewari S. Optimization of hetero-gate-dielectric tunnel FET for label-free detection and identification of biomolecules. *IEEE Trans Electron Devices* (2020) 67(5):2157–64. doi:10.1109/TED.2020.2978499

2. Dwivedi P, Singh R. Investigation the impact of the gate work-function and biases on the sensing metrics of TFET based biosensors. *Eng Res Express* (2020) 2(2):25043. doi:10.1088/2631-8695/ab9bf0

3. C R, Jr, Lyons C. Electrode systems for continuous monitoring in cardiovascular surgery. *Ann NY Acad Sci* (1962) 102:29–45. doi:10.1111/j.1749-6632.1962.tb13623.x

4. Dutta R, Sarkar SK. Analytical modeling and simulation-based optimization of broken gate TFET structure for low power applications. *IEEE Trans Electron Devices* (2019) 66(8):3513–20. doi:10.1109/TED.2019.2925109

5. Zheng B, Li D, Zhu C, Lan J, Sun X, Zheng W, et al. Dual-channel type tunable field-effect transistors based on vertical bilayer WS2 (1- X) Se2 x/SnS2 heterostructures. *InfoMat* (2020) 2(4):752–60. doi:10.1002/inf2.12071

6. Li J, Li L, Zhao P, Xie Y, zhao J. Ultrasensitive electrochemical sensor for fenitrothion based on MIL-125 derived iron/titanium bimetallic oxides doped porous carbon composite. *Microchemical J* (2024) 200:110426. and others. doi:10.1016/j.microc.2024.110426

7. Li D, Yin J, Yu Z, Gao Z, Xu N, Meng L. Artificial intelligence-assisted colorimetric sensor array based on supramolecular self-assembled nanozymes for visual monitoring of pesticide residues. *Sens Actuators B Chem* (2025) 444:138493. doi:10.1016/j.snb.2025.138493

8. Tang Y, Li Y, Chen P, Zhong S, Yang Y. Nucleic acid aptamer-based sensors for bacteria detection: a review. *BioEssays* (2025) 47(3):e202400111. doi:10.1002/bies.202400111

9. Liu G, Guan X, Zhang P, Tan Q, Li T, Jin X, et al. A fully integrated wearable microfluidic electrochemical sensor with ultrasonic connecting and hot-pressing bonded multilayer structure for sweat biomarker analysis. *Anal Chem* (2025) 97(41):22858–70. doi:10.1021/acs.analchem.5c04641

10. Chen Z, Li J, Li T, Fan T, Meng C, Li C, et al. A CRISPR/Cas12a-empowered surface plasmon resonance platform for rapid and specific diagnosis of the omicron variant of SARS-CoV-2. *Natl Sci Rev* (2022) 9(8):nwac104. doi:10.1093/nsr/nwac104

11. Barbaro M, Bonfiglio A, Raffo L. A charge-modulated FET for detection of biomolecular processes: conception, modeling, and simulation. *IEEE Trans Electron Devices* (2005) 53(1):158–66. doi:10.1109/ted.2005.860659

12. Kim C-H, Jung C, Park HG, Choi Y-K. Novel dielectric modulated field-effect transistor for label-free DNA detection. *Biochip J* (2008) 2(2):127–34.

13. Wangkheirakpam VD, Bhowmick B, Pukhrambam PD. Near-infrared optical sensor based on band-to-band tunnel FET. *Appl Phys A* (2019) 125(5):341. doi:10.1007/s00339-019-2636-3

14. Chanda M, Das R, Kundu A, Sarkar CK. Analytical modeling of label free biosensor using charge plasma based gate underlap dielectric modulated MOSFET. *Superlattices Microstruct* (2017) 104:451–60. doi:10.1016/j.spmi.2017.03.010

15. Kim C-H, Jung C, Lee K-B, Park HG, Choi Y-K. Label-free DNA detection with a nanogap embedded complementary metal oxidesemiconductor. *Nanotechnology* (2011) 22(13):135502. doi:10.1088/0957-4484/22/13/135502

16. Vishnoi R, Kumar MJ. A compact analytical model for the drain current of gate-all-around nanowire tunnel FET accurate from sub-threshold to ON-state. *IEEE Trans Nanotechnol* (2015) 14(2):358–62. doi:10.1109/tnano.2015.2395879

17. Hafiz SA, Ehteshamuddin M, Loan SA. And others, "Dielectrically modulated source-engineered charge-plasma-based Schottky-FET as a label-free biosensor,". *IEEE Trans Electron Devices* (2019) 66(4):1905–10. doi:10.1109/TED.2019.2896695

18. Sarkar D, Banerjee K. Proposal for tunnel-field-effect-transistor as ultra-sensitive and label-free biosensors. *Appl Phys Lett* (2012) 100(14):143108. doi:10.1063/1.3698093

19. Gao A, Lu N, Wang Y, Li T. Robust ultrasensitive tunneling-FET biosensor for point-of-care diagnostics. *Sci Rep* (2016) 6(1):22554. doi:10.1038/srep22554

20. Wang Y, Li C, Li O, Cheng S, Liu W, You H. Simulation study of dual metal-gate inverted T-shaped TFET for label-free biosensing. *IEEE Sens J* (2022) 22(19):18266–72. doi:10.1109/jsen.2022.3195180

21. Priyadarshani KN, Singh S. Ultra sensitive label-free detection of biomolecules using vertically extended drain double gate $Si_{0.5}Ge_{0.5}$ source tunnel FET. *IEEE Trans Nanobioscience* (2021) 20(4):480–7. doi:10.1109/TNB.2021.3106333

22. Rashid S, Bashir F, Khanday FA, Rafiq Beigh M. Dielectrically modulated III-V compound semiconductor based pocket doped tunnel FET for label free biosensing applications. *IEEE Trans Nanobioscience* (2023) 22(1):192–8. doi:10.1109/TNB.2022.3178763

23. Dwivedi P, Kranti A. Applicabilityof Transconductance-to-CurrentRatio(gm/Ids)asaSensingMetricforTunnelFET biosensors. *IEEE Sens J* (2017) 17(4):1030–6. doi:10.1109/JSEN.2016.2640192

24. Kanungo S, Chattopadhyay S, Gupta PS, Rahaman H. Comparative performance analysis of the dielectrically modulated full-gate and short-gate tunnel FET-Based biosensors. *IEEE Trans Electron Devices* (2015) 62(3):994–1001. doi:10.1109/ted.2015.2390774

25. Kanungo S, Chattopadhyay S, Gupta PS, Sinha K, Rahaman H. Study and analysis of the effects of SiGe source and pocket-doped channel on sensing performance of dielectrically modulated tunnel FET-Based biosensors. *IEEE Trans Electron Devices* (2016) 63(6):2589–96. doi:10.1109/ted.2016.2556081

26. Abdi DB, Kumar MJ. Dielectric modulated overlapping gate-on-drain tunnel-FET as a label-free biosensor. *Superlattices Microstruct* (2015) 86:198–202. doi:10.1016/j.spmi.2015.07.052

27. Narang R, Saxena M, Gupta RS, Gupta M. Dielectric modulated tunnel field-effect transistor—A biomolecule sensor. *IEEE Electron Device Letters* (2011) 33(2):266–8. doi:10.1109/led.2011.2174024

28. Nair PR, Alam MA. Design considerations of silicon nanowire biosensors. *IEEE Trans Electron Devices* (2007) 54(12):3400–8. doi:10.1109/ted.2007.909059

29. Silvaco I. ATLAS user's manual: device simulation software, *Silvaco Int*. Santa Clara, CA, USA (2018).

30. Boucart K, Ionescu AM. Double-gate tunnel FET with high-k gate dielectric. *IEEE Trans Electron Devices* (2007) 54(7):1725–33. doi:10.1109/ted.2007.899389

31. Dwivedi P, Singh R, Sengar BS, Kumar A, Garg V. A new simulation approach of transient response to enhance the selectivity and sensitivity in tunneling field effect transistor-based biosensor. *IEEE Sens J* (2020) 21(3):3201–9. doi:10.1109/jsen.2020.3028153

32. Venkatesh P, Nigam K, Pandey S, Sharma D, Kondekar PN. A dielectrically modulated electrically doped tunnel FET for application of label free biosensor. *Superlattices Microstruct* (2017) 109:470–9. doi:10.1016/j.spmi.2017.05.035

33. Singh R, Kaim S, MedhaShree R, Kumar A, Kale S. Dielectric engineered schottky barrier MOSFET for biosensor applications: proposal and investigation. *Silicon* (2022) 14(8):4053–62. doi:10.1007/s12633-021-01191-4

34. Yan J, Kang Y, Fang W, Zhu B, Song Z. Tuning gas sensing properties through metal-nanocluster functionalization of 3D SnO2 nanotube arrays for selective gas detection. *ACS Sens* (2025) 10(8):6084–94. doi:10.1021/acssensors.5c01699

35. He Y, Yuan M, Li Q, Tang L, Yang W, Ping Y, et al. Feasibility study of mechanical stress wave detection in power semiconductor devices using bare FBG sensors. *IEEE Sens J* (2025) 25:39849–57. doi:10.1109/jsen.2025.3615108

36. Zhang Y, Wang Y, Su C, Miao Y, Wei T, Feng Y, et al. Multi-sensor fusion-based intelligent auxiliary system of power wheelchairs for individuals with limbs disabilities: design and implementation. *Measurement* (2025) 257:118573. doi:10.1016/j.measurement.2025.118573

37. Du B, Tian X, Chen Z, Ge Y, Chen C, Gao H, et al. Ultrasensitive optoelectronic biosensor arrays based on twisted bilayer graphene superlattice. *Natl Sci Rev* (2025) 12(10):nwaf357. doi:10.1093/nsr/nwaf357